7-17-2021

Hydrochloric acid modification and lead removal studies on naturally occurring zeolites from Nevada, New Mexico, and Arizona

Garven M. Huntley
Michigan Technological University, gmhuntle@mtu.edu

Rudy Luck
Michigan Technological University, rluck@mtu.edu

Michael Mullins
Michigan Technological University, memullin@mtu.edu

Nick Newberry
Michigan Technological University, nknewber@mtu.edu

processes

MDPI

Article

Hydrochloric Acid Modification and Lead Removal Studies on Naturally Occurring Zeolites from Nevada, New Mexico, and Arizona

Garven M. Huntley [1], Rudy L. Luck [1,*], Michael E. Mullins [2] and Nick K. Newberry [1]

[1] Department of Chemistry, Michigan Technological University, 1400 Townsend Drive, Houghton, MI 49931, USA; gmhuntle@mtu.edu (G.M.H.); Nknewber@mtu.edu (N.K.N.)
[2] Department of Chemical Engineering, Michigan Technological University, 1400 Townsend Drive, Houghton, MI 49931, USA; memullin@mtu.edu
* Correspondence: rluck@mtu.edu; Tel.: +1-906-487-7137; Fax: +1-906-487-2061

Abstract: Four naturally occurring zeolites were examined to verify their assignments as chabazites AZLB-Ca and AZLB-Na (Bowie, Arizona) and clinoptilolites NM-Ca (Winston, New Mexico) and NV-Na (Ash Meadows, Nevada). Based on powder X-ray diffraction, NM-Ca was discovered to be mostly quartz with some clinoptilolite residues. Treatment with concentrated HCl (12.1 M) acid resulted in AZLB-Ca and AZLB-Na, the chabazite-like species, becoming amorphous, as confirmed by powder X-ray diffraction. In contrast, NM-Ca and NV-Na, which are clinoptilolite-like species, withstood boiling in concentrated HCl acid. This treatment removes calcium, magnesium, sodium, potassium, aluminum, and iron atoms or ions from the framework while leaving the silicon framework intact as confirmed via X-ray fluorescence and diffraction. SEM images on calcined and HCl treated NV-Na were obtained. BET surface area analysis confirmed an increase in surface area for the two zeolites after treatment, NM-Ca 20.0(1) to 111(4) m^2/g and NV-Na 19.0(4) to 158(7) m^2/g. ^{29}Si and ^{27}Al MAS NMR were performed on the natural and treated NV-Na zeolite, and the data for the natural NV-Na zeolite suggested a Si:Al ratio of 4.33 similar to that determined by X-ray fluorescence of 4.55. Removal of lead ions from solution decreased from the native NM-Ca, 0.27(14), NV-Na, 1.50(17) meq/g compared to the modified zeolites, 30 min HCl treated NM-Ca 0.06(9) and NV-Na, 0.41(23) meq/g, and also decreased upon K^+ ion pretreatment in the HCl modified zeolites.

Keywords: clinoptilolites; acid modification; heavy metals; toxic substances; purification; lead removal

Citation: Huntley, G.M.; Luck, R.L.; Mullins, M.E.; Newberry, N.K. Hydrochloric Acid Modification and Lead Removal Studies on Naturally Occurring Zeolites from Nevada, New Mexico, and Arizona. *Processes* **2021**, *9*, 1238. https://doi.org/10.3390/pr9071238

Academic Editors: Monika Wawrzkiewicz and Anna Wołowicz

Received: 15 June 2021
Accepted: 13 July 2021
Published: 17 July 2021

1. Introduction

Natural zeolites, which are composed of hydrated aluminosilicates containing group I and II metals [1], are an abundant resource [2], with desirable chemical properties for many different applications, such as in construction [3], slow release of fertilizer [4–10], cosmetics [11], reduction of lactate or ammonia in mammalian blood [12], removal of Fe and Mn from water [13], catalysis and ion exchange [14], and in environmental protection [15]. Zeolites have a crystalline structure with small voids, commonly called pores, that act as a site for the zeolite to capture or stabilize different cations or molecules. These compounds have been utilized to remove salinity/sodicity [16], copper [17], Cr^{6+} [18], Mn^{2+} [19], heavy metals [20], ammonia [21], phosphorus [22], purify urine [23], zinc [24] from wastewater, and also anions such as Cl^- and CO_3^{2-} [25]. Zeolites contain cations to stabilize the negative charge in their structure, with Na^+, K^+, Ca^{2+}, and Mg^{2+} being the four most common with others possible [26]. While it is possible to synthesize a single phase of clinoptilolite [27], as much as 4.75 mg Fe/g of Mexican natural zeolite consisting of clinoptilolite, mordenite, and feldspar phases was reported [28].

During the ion exchange process, zeolites adsorb toxic metal ions dissolved in solutions into their pores while releasing the other cations present in the structure into the

solutions. Thus, water contaminated with Pb^{2+} ions, which are toxic to humans, could be made safe by stirring with a zeolite to remove the Pb^{2+} ions from the solution. The Pb^{2+} ions would be contained inside the zeolite and could be easily filtered off, and the Na^{+} ion that was previously in the zeolite would now be dissolved in the water, rendering it safer for human consumption [29].

In this report, four naturally occurring zeolites that were reported to be of the chabazite and clinoptilolite (based on Si:Al $\geq$ 4.0 [30]) varieties were examined [31]. The chabazite form has been explored for its unusually high-sodium composition [32] and chemical upgrading [33], and the clinoptilolite zeolite has been studied for various membrane applications [34–36]. Additionally, both chabazite and clinoptilolite were previously subjected to treatment with base and applied for Pb^{2+} and Cd^{2+} removal [37]. It was of some interest to determine if modifications under acidic conditions while maintaining structural integrity were possible and what impact this would have on their properties and potential use in remediation, an idea prompted by a publication on chemical etching on a glass surface using HCl [38]. A report dealing with the treatment of naturally occurring clinoptilolites in Cuba using 0.6 M HCl discovered that milder forms of acid treatment were required as higher concentrations led to the decomposition of the zeolites [39]. Another report found that the basic clinoptilolite structure remained after acid leaching and heating to 600 °C [40].

In the present study, the integrity of the samples, i.e., their purity and classification as chabazite and clinoptilolite, was assessed as evident by powder X-ray diffraction. Additionally, treatment with concentrated HCl removes metal ions from the pores leaving the silicon framework intact with the clinoptilolite variety, whereas the chabazite ones became amorphous. A variety of analytical techniques were employed to assess the nature and composition of the natural and acid-modified zeolites, including solid-state ^{29}Si and ^{27}Al NMR, BET measurements [41], SEM images, and powder X-ray fluorescence and diffraction. Lead removal studies on the clinoptilolite samples suggested differing capacities between the two samples after calcination and deterioration of Pb^{2+} storage capacity upon modification.

The following abbreviations are used.

APD—$AlPO_4$-D, a tetrahedrally coordinated aluminophosphate zeolite framework
ATR—FTIR-Attenuated Total Reflectance-Fourier Transformed Infrared spectroscopy
BET—Brunauer Emmett Teller
CHA—chabazite
CLI—clinoptilolite
EDS/XRF—energy dispersive X-ray spectroscopy/X-ray fluorescence
ERI—erionite
HCl—hydrochloric acid
MAS—magic angle spinning
NMR—nuclear magnetic resonance
SEM—scanning electron microscope

2. Materials and Methods

2.1. Materials

The zeolites were generously donated from the St. Cloud Mining Company and consisted of St. Cloud Mining Bowie chabazite (AZLB-Na, −325 mesh), St. Cloud Mining Bowie chabazite (AZLB-Ca, −325 mesh), St. Cloud Winston clinoptilolite (NM-Ca, −325 mesh), and St. Cloud Mining Ash Meadows clinoptilolite (NV-Na, −325 mesh), where AZLB = Arizona Land Basin, NM = New Mexico, NV = Nevada, Na is the dominant cation, and Ca is the dominant cation. HCl (12.1 M) and HNO_3 (15.6 M) acids were obtained from Fisher. Lead nitrate was obtained from Mallinckrodt Chemical Works.

2.1.1. Zeolite Modifications

Calcined Zeolites

The calcined zeolite samples were obtained by heating the zeolites at 550 °C for 5 h under air. After cooling the zeolite, the samples were stored in a desiccator to prevent the absorption of water.

Hydrochloric Acid Treated Zeolites

The HCl acid-treated samples were prepared by heating at 85 °C a solution of the acid and zeolite at a ratio of 10 mL of concentrated HCl (12.1 M) per gram of zeolite. This was based on a procedural modification from the literature [38], and the samples were placed in an oil bath for 10, 20, 30, or 40 min and, upon removal, allowed to cool for 20 min. The zeolite was quickly filtered off after cooling and washed with water three times at a ratio of 5 mL per gram of zeolite initially used. The final rinse was clear as assessed with pH paper, and when added to solutions of $AgNO_3$ did not result in a white (i.e., AgCl) precipitate. The zeolite was dried overnight in an oven at 70 °C and then calcined at 550 °C in a flow of air for 5 h. After cooling, the zeolite was stored in a desiccator to prevent the absorption of water.

2.2. Methods

2.2.1. X-ray Diffraction

X-ray diffraction spectra of the zeolites were collected using a Scintag XDS 2000 Diffractometer (Scintag Inc., Division of Thermo, Dearborn, MI, USA) using a copper target to generate X-rays and a graphite monochromator with a scan range of 5–60° 2θ, a step size of 0.020°, a count time of 0.600 s, and a step scan rate of 2.0 deg/min. The samples were packed into an aluminum sample plate of dimensions of 30 mm wide by 90 mm long by 8 mm depth.

The data were analyzed using the program DMSNT v 1.37 (1994–1998) Scintag Inc. (Division of Thermo, Dearborn, MI, US). The spectra were background-subtracted using a manual spline curve fit. Sample phase identification was conducted using QualX2 [42] after the raw data was transformed using PowDLL [43].

2.2.2. Surface Area Analysis

Surface area analysis was performed using an ASAP 2020 machine made by Micrometrics (Norcross, GA, USA). The program used for the analysis was the "5-point BET Analysis" program supplied by the manufacturer. Some modifications were required and consisted of adding parameters from the standard micropore analysis program (from the manufacturer) to the 5 Point BET Program. The samples were degassed at 350 °C at 1 mm Hg for 4 h and backfilled with nitrogen gas. The BET analysis was performed using nitrogen gas, and the micropore analysis was performed using helium gas. Calibration of the machine was checked by running a standard supplied by Micrometrics.

2.2.3. Energy Dispersive Spectroscopy

EDS/XRF was performed to obtain an elemental composition of the zeolites using a Xenemetrix EX-6600 EDS machine (Migdal HaEmek, Israel) with a rhodium target to generate the X-rays. Samples were prepared by mixing the zeolite with corn starch at a ratio of 4:1 weight zeolite:corn starch. The mixture was added to an aluminum cup with a diameter of 3 cm and a depth of 0.75 cm. Once packed by hand pressure, the cup was loaded into a hydraulic press and pressure applied for 1 min up to 700 psi; once reached, the sample was held for 1 min at 700 psi, and then for 1 min, the pressure was released.

2.2.4. NMR Study of Zeolite

^{27}Al MAS and ^{29}Si MAS NMR analyses of calcined NV-Na and 30 min HCl NV-Na were performed at ambient temperature on a Varian Infinity-Plus NMR spectrometer equipped with a 6 mm MAS broadband probe operating at 79.41 MHz for ^{29}Si, 104.2 MHz

for ^{27}Al, and 399.75 MHz for ^{1}H. Samples were spun at the magic angle at 4 kHz. A standard one-pulse was used for all experiments. The ^{29}Si pulse width was 4 μs, the pulse delay was 120 s, the acquisition length was 20.5 ms, and between 650 and 700 scans were collected. Exponential multiplication of 100 Hz was used before the Fourier transform. Chemical shifts were referenced against an external sample of talc at −98.1 ppm relative to TMS (tetramethylsilane) at 0 ppm. The ^{27}Al pulse width was 1 μs, the pulse delay was 0.2 s, the acquisition length was 2.1 ms, and between 8000 and 10,000 scans were collected. Exponential multiplication of 100 Hz was used prior to the Fourier transform. Chemical shifts were referenced against an external sample of 1M $Al(NO_3)_3$ at 0.0 ppm.

2.2.5. Scanning Electron Microscopy

SEMs were performed on uncoated samples (loaded onto double-sided carbon tape followed by air removal of unstuck material) using a Hitachi S4700 scanning electron microscope at a voltage of 15–20 kV and 10–20 μA.

2.2.6. ATR-FTIR

ATR-FTIR spectroscopy was performed on pure material using calcined and modified pulverized samples on a PerkinElmer Spectrum one with a Perkin Elmer universal ATR sampling attachment.

2.2.7. Lead Removal Studies

An analysis of the amount of lead absorbed or adsorbed by the zeolite was performed using a Buck Scientific Model 200 A atomic absorption spectrometer. A Fisher hollow cathode tube for lead analysis was used at an operating current of 10 mA. The detector was set to a wavelength of 283.3 nm with a slit width of 0.7 nm.

A 335 mg/L concentrated lead nitrate solution was made using water with a pH of 4.5, which was adjusted using HNO_3 acid. A total of 0.250 g of previously dried zeolite was added to 150 mL of the 335 ppm lead nitrate solution and stirred for 5 days at room temperature as detailed previously [44]. After 5 days, the solution was centrifuged, the sample was diluted, and analysis was performed on the AAS.

2.2.8. Flow Chart of Techniques

The techniques utilized in this paper are illustrated in Scheme 1.

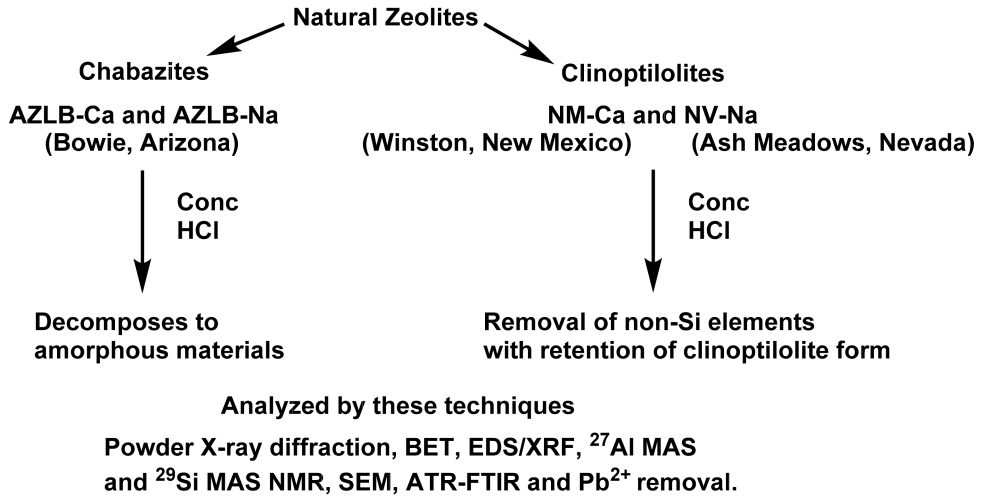

Scheme 1. Flow chart summarizing results and listing utilized analytical techniques.

3. Results and Discussion

3.1. X-ray Diffraction

Initial Phase Assignment

The spectra obtained for AZLB-Ca, Figure 1, and AZLB-Na, Figure 2, suggests the presence of chabazite if one compares the patterns to that obtained from simulations [45] of single-crystal X-ray data [21]. In particular, present were intense reflections for Miller indices (1 0 0) and (3 $\bar{1}$ $\bar{1}$) at 2θ of 9.40 and 30.40°, respectively, which are ascribed to chabazite [45]. These suggest that the samples were dominantly chabazite; however, differing ratios of erionite and $AlPO_4$-D were also evident in the samples [45,46]. Interestingly, no phases indicative of clinoptilolite, heulandite, or alpha quartz were observed in either sample AZLB-Ca or AZLB-Na, Figure 1 and Figure 2, respectively.

The X-ray powder spectra for the clinoptilolite samples, NV-Na Figure 3 and NM-Ca Figure 4, also contained large differences. Evidence for clinoptilolites is in the presence of reflections at 9.88, 11.19, and 22.49° in 2θ ascribable to the (0 2 0), (2 0 0), and (3 3 0) Miller indices respectively [45,47,48]. In the case of the calcined NV-Na sample (Figure 3a), signals for these peaks are quite intense, and the sample appears to be quite pure. There was a match for clinoptilolite-Na (card [00-900-1391]) at an FoM of 0.75 determined using QualX2 [42] (Figure 3b). Raw data from the diffractometer were converted with PowDLL [43] for use with the QualX2 program. In the case of NM-Ca (Figure 4), the most intense peak is located at about a 2θ of 26.6°, and the program QualX2 [42] could not find a match to clinoptilolite. This is probably because this calcined NM-Ca sample is mostly alpha quartz, which has its most intense reflection at a 2θ of 26.65° due to the (1 0 1) Miller phase [49]. There is some evidence of clinoptilolite in the sample judging by small peaks at the 2θ angles mentioned above, but it is clearly not the dominant constituent. No chabazite or erionite species were observed in either sample NV-Na or NM-Ca.

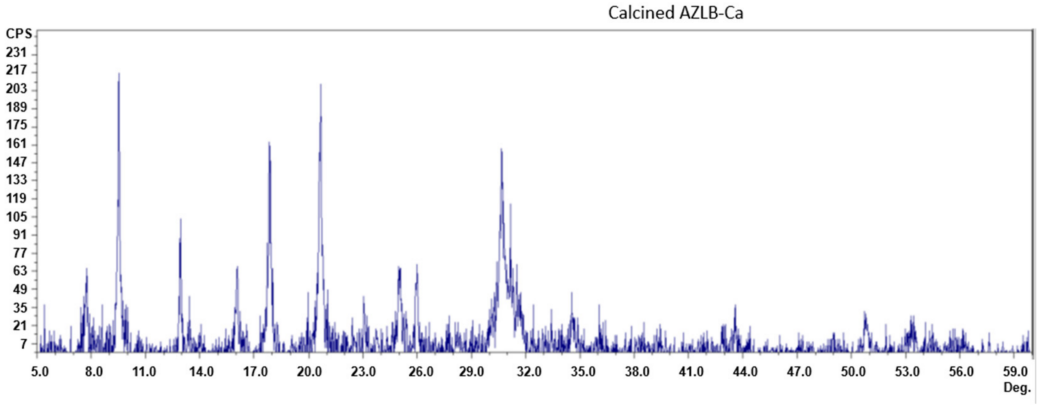

Figure 1. The XRD pattern of calcined AZLB-Ca.

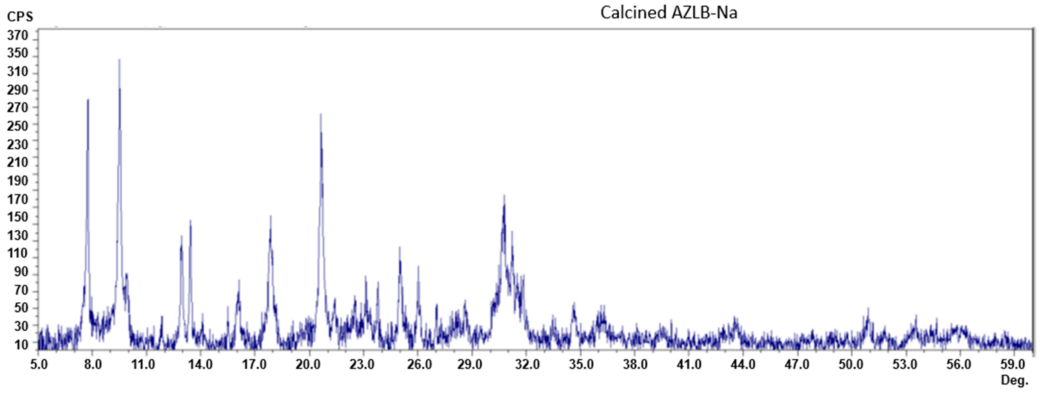

Figure 2. The XRD pattern of calcined AZLB-Na.

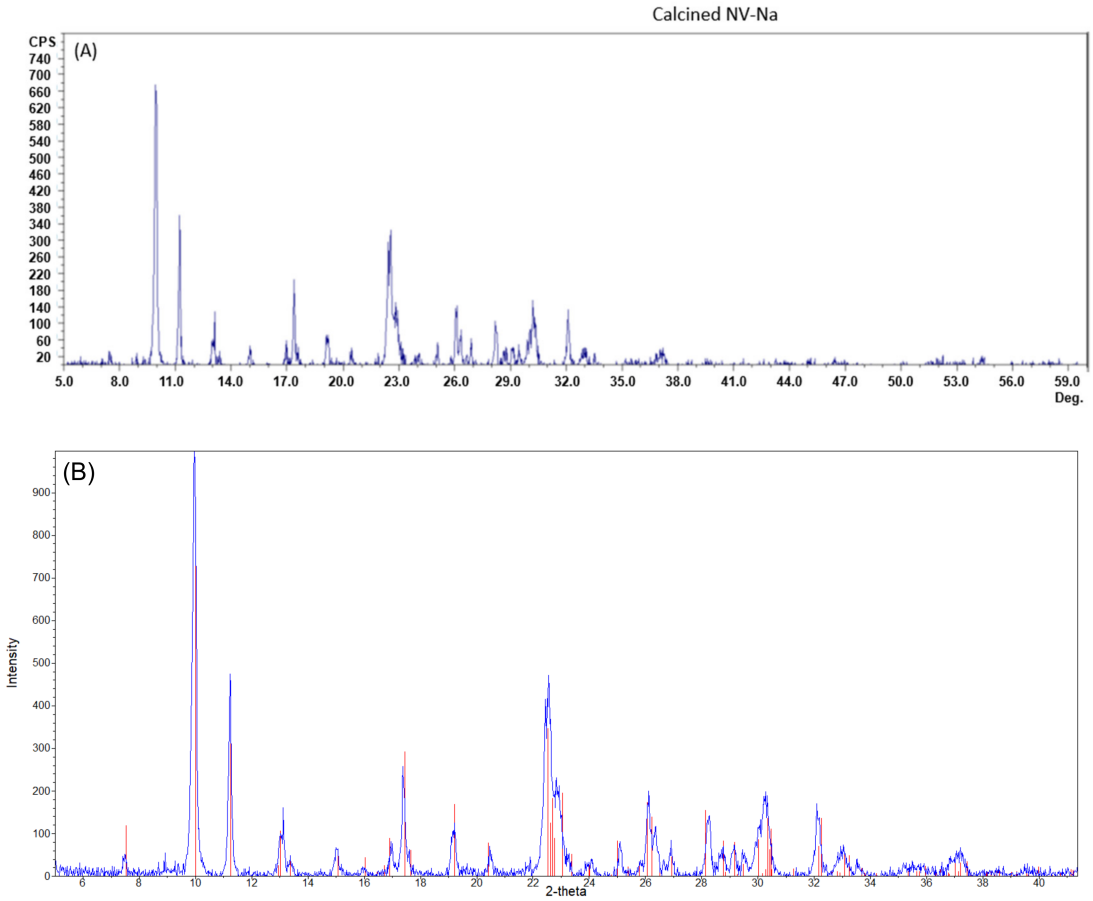

Figure 3. ((**A**), above) The XRD pattern of calcined NV-Na. ((**B**), below) An expanded drawing of the XRD pattern for calcined NV-Na illustrated using QualX2 [42]. Solid vertical lines represent card [00-900-1391] clinoptilolite-Na at an FoM of 0.75. Raw data converted with PowDLL [43].

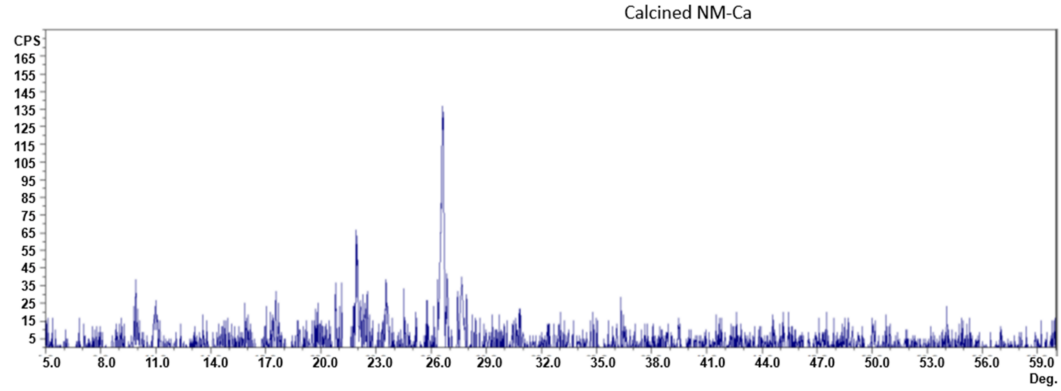

Figure 4. The XRD pattern of calcined NM-Ca.

The AZLB-Na and AZLB-Ca zeolites lost all crystallinity when boiled in HCl acid for 30 min, which is demonstrated by the loss of all sharp reflections and the spectra appearing as broad bumps (Figures 5 and 6) as a result of random scattering due to an amorphous material. In contrast, the NV-Na and NM-Ca zeolites did not lose all crystallinity during the boiling process in HCl acid (Figure 7 and Figure 8, respectively). This is conclusive evidence of the instability of these chabazites subjected to HCl modification and the inherent stability of the clinoptilolites as evident in the 30 min HCl NV-Na, Figure 7, card [00-900-1393] clinoptilolite-Na at an FoM of 0.66, and 30 min HCl NM-Ca, Figure 8, card

[00-901-4410] boggsite [50] of formula $Ca_{3.4}O_{70.76}Si_{24}$ at an FoM of 0.77, both determined using QualX2 [42]. In particular, NM-Ca registered the least change possible because it is mostly composed of alpha quartz, Figure 8.

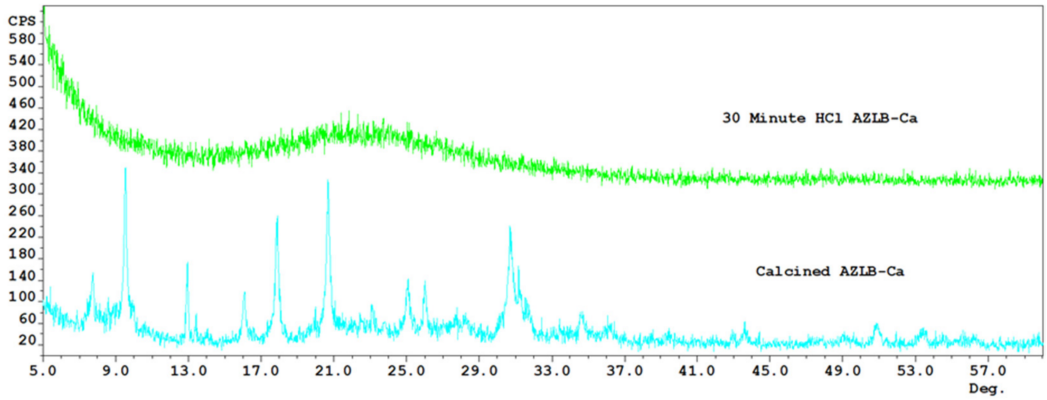

Figure 5. The XRD patterns of calcined AZLB-Ca and 30 min HCl AZLB-Ca.

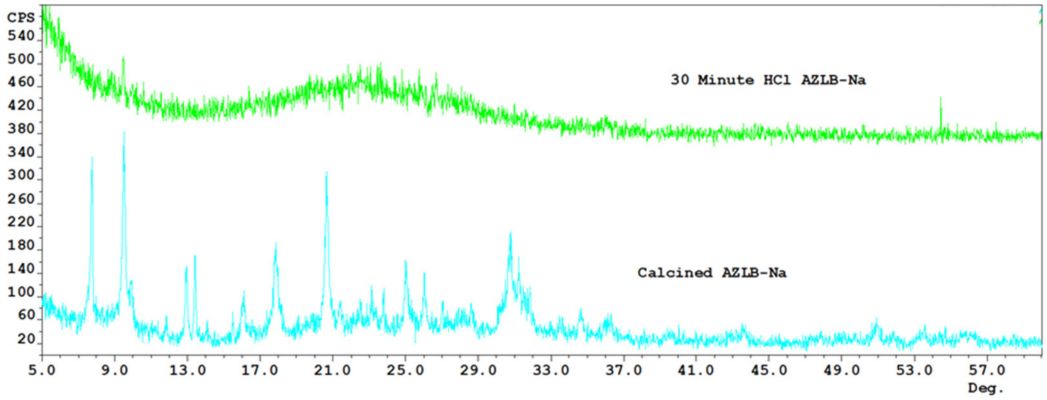

Figure 6. The XRD patterns of calcined AZLB-Na and 30 min HCl AZLB-Na.

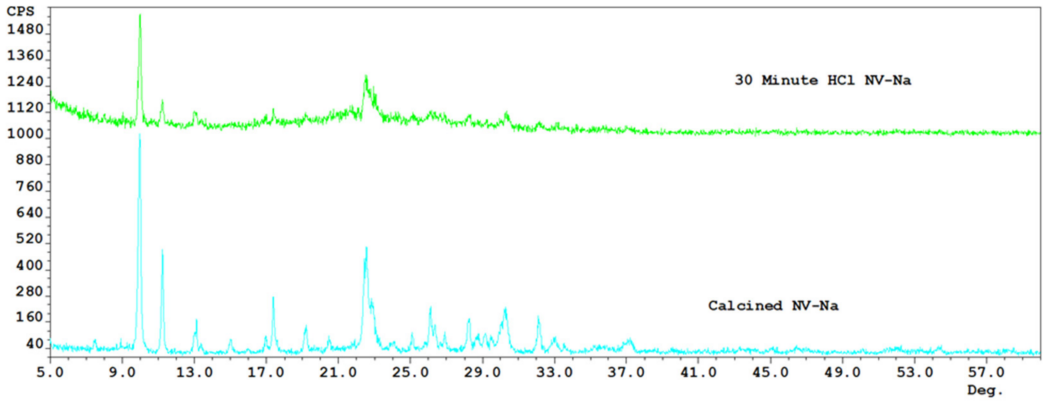

Figure 7. The XRD patterns of calcined NV-Na and the 30 min HCl NV-Na.

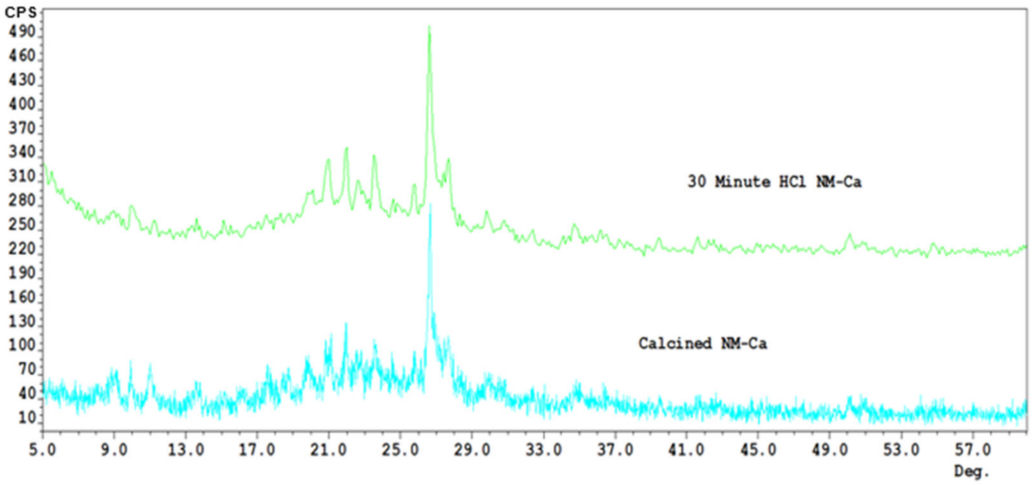

Figure 8. The XRD patterns of calcined NM-Ca and 30 min HCl NM-Ca.

3.2. Surface Area Analysis

Based on the fact that the chabazite samples lost crystallinity upon treatment with conc. HCl, only surface area analyses on the clinoptilolite samples were conducted. Thus NM-Ca and NV-Na were both subjected to boiling concentrated HCl acid for a varying amount of time from 10 to 40 min, as listed with the surface area analysis results (Table 1). This indicated that 30 min etching of the zeolite produced the highest surface area, with 40 min etching resulting in a decrease in the surface area, which is likely due to the acid collapsing some of the crystalline structure. Therefore, in this case, the optimum time for boiling the clinoptilolite zeolite in HCl acid is 30 min. In the case of NV-Na, the surface area increased from 19 to 158 m^2/g, and the pore volume increased from 0.04 to 0.12 cm^3/g. The NM-Ca increased in surface area from 20 to 111 m^2/g, and the pore volume increased from 0.04 to 0.10 cm^3/g.

The values for the micropore, mesopore, and external surface areas provide valuable insight into what is happening during the etching process, Tables 1 and 2. There is a dramatic increase in micropore area of the HCl acid-etched zeolites, 4.800 to 94.99 m^2/g for calcined NV-Na to 30 min HCl NV-Na, and 2.730 to 55.15 m^2/g for calcined NM-Ca to 30 min HCL NM-Ca, suggesting that either new micropores are forming and/or the existing micropores are being deepened, increasing their surface area. In the case of the calcined NM-Ca sample versus the 10 min HCl NM-Ca sample, Table 2, the 10 min HCl NM-Ca sample has a smaller average micropore diameter going from 4.584 to 4.388 Å, and this likely represents new micropores being formed, thus lowering the average value for the micropore diameter. The 30 min HCl NM-Ca sample seems to reach a maximum average micropore diameter of 4.597 Å before declining in the 40 min HCl NM-Ca sample to 4.588 Å, which is probably due to the crystallinity of the zeolite collapsing based on the loss of surface area of the sample, see Table 1. In contrast, NV-Na appears less stable to HCl treatment, and the average micropore diameter increases from 4.586 to 4.600 Å for calcined NV-Na to 30 min HCl NV-Na, respectively.

In the case of mesopores, calcined NV-Na has a value of 91.00 Å, which decreases to 31.06 Å in the 10 min HCl NV-Na sample. This is attributable to the formation of new mesopores, thus lowering the average diameter of mesopores. The same trend is observed with the calcined NM-Ca sample, which has an initial average mesopore diameter of 93.71 Å (calcined NM-Ca), and changes to 40.31 Å (10 min HCl NM-Ca sample). In the case of the NM-Ca zeolite, the average mesopore diameter continues to become lower with longer treatment in HCl acid. However, the NV-Na zeolite reaches equilibrium around a 32 Å average mesopore diameter (Table 2).

Table 1. The surface area analysis measurements for calcined and HCl etched zeolites.

Sample	5 Point BET Surface Area (m^2/g)	Pore Volume (cm^3/g)	Micropore Volume (cm^3/g)	Micropore Area (m^2/g)	External Surface Area (m^2/g)
NV-Na calcined	19.0(4)	0.04	0.002	4.8	14.23
10 min HCl NV-Na	147(6)	0.11	0.049	93.28	52.05
20 min HCl NV-Na	141(6)	0.11	0.043	81.43	59.87
30 min HCl NV-Na	158(7)	0.12	0.051	94.99	63.15
40 min HCl NV-Na	138(6)	0.11	0.041	75.06	63.49
NM-Ca calcined	20.0(1)	0.04	0.001	2.73	17.27
10 min HCl NM-Ca	82.0(3)	0.08	0.021	38.71	43.36
20 min HCl NM-Ca	89.0(3)	0.08	0.022	41.61	47.75
30 min HCl NM-Ca	111(4)	0.1	0.029	55.15	56.22
40 min HCl NM-Ca	101(4)	0.08	0.028	53.53	48.28

Table 2. The average mesopore and micropore diameter.

Sample	Average Micropore Diameter (Å)	Average Mesopore Diameter (Å)
NV-Na calcined	4.586	91.00
10 min HCl NV-Na	4.597	31.06
20 min HCl NV-Na	4.591	32.44
30 min HCl NV-Na	4.600	31.72
40 min HCl NV-Na	4.598	32.95
NM-Ca calcined	4.584	93.71
10 min HCl NM-Ca	4.388	40.31
20 min HCl NM-Ca	4.584	39.62
30 min HCl NM-Ca	4.597	36.36
40 min HCl NM-Ca	4.588	34.63

3.3. X-ray Fluorescence/EDS

The NM-Ca zeolite has a much greater mole percentage concentration of Ca (6.31%) compared to that for NV-Na (1.14%) while containing less Na (0.10 to 0.25, respectively), clearly justifying the label, Table 3. There is also more Fe in NM-Ca compared to NV-Na (2.67 to 0.79%, respectively) and correspondingly less Si (76.26 to 84.36%, respectively). The X-ray fluorescence data results in Table 3 show, by way of the reduction in molar percentage concentrations, that etching the zeolites in concentrated HCl acid effectively removes sodium, calcium, potassium, magnesium, iron, and aluminum, while the silicon concentration increases proportionally. Table 4 lists the weight percentage data supplied by the manufacturer [31] and that obtained by converting the molar percentages in Table 3 to weight percentages. This requires the assumption that only the ions listed in Table 3 were present and are also present in the zeolite in the oxide form indicated in the table. Additionally, XRF is not good at determining very low concentrations. However, there are large differences in the weight percentages between our determinations and those determined by the manufacturer. This may well be due to natural variation in the samples used in the studies. Our determinations of the concentrations of Al_2O_3 would appear to be much lower, whereas those for SiO_2 are higher compared to those listed by the manufacturer. However, this does correlate with the X-ray powder diffraction pattern where quartz was found in NM-Ca, Figure 8. On this basis, NV-Na is composed mostly of K_2O, Al_2O_3, and SiO_2, in contrast to NM-Ca, where CaO, K_2O, Fe_2O_3, Al_2O_3, and SiO_2 are the major contributors. This calculation allows for a stoichiometric formula for NV-Na of $[Na_2O]_{0.01}[CaO]_{0.11}[K_2O]_{0.27}[MgO]_{0.02}[Fe_2O_3]_{0.11}[P_2O_5]_{0.05}[Al_2O_3]_{0.80}[SiO_2]_{8.63}$ and NM-Ca of $[CaO]_{0.60}[K_2O]_{0.34}[MgO]_{0.04}[Fe_2O_3]_{0.36}[Al_2O_3]_{0.83}[SiO_2]_{7.79}$.

Table 3. The XRF data for zeolites in mole %.

Experimental Run	Na	Ca	K	Mg	Fe	Al	Si	P	Si: Al_2 Ratio
NV-Na	0.25 ± 0.08	1.14 ± 0.04	3.34 ± 0.08	0.30 ± 0.08	0.79 ± 0.01	9.27 ± 0.24	84.36 ± 0.70	0.442 ± 0.08	4.55
30 min NV-Na	0.02 ± 0.04	0.05 ± 0.01	0.30 ± 0.02	0.16 ± 0.04	0.04 ± 0.002	4.16 ± 0.11	95.04 ± 0.49	0.17 ± 0.03	11.42
NM-Ca	0.10 ± 0.04	6.31 ± 0.11	4.29 ± 0.10	0.52 ± 0.05	2.67 ± 0.04	9.51 ± 0.17	76.26 ± 0.46	0.27 ± 0.04	4.01
30 min NM-Ca	0.04 ± 0.04	0.42 ± 0.04	2.54 ± 0.08	0.17 ± 0.05	0.07 ± 0.002	4.71 ± 0.13	91.83 ± 0.56	0.17 ± 0.04	9.75

Table 4. The weight percentages from our calculated data and that of the manufacturer.

			NV-Na		NM-Ca	
Experimental	**Mole %**	**Formula**	**Calculated**	**Manufacturer**	**Calculated**	**Manufacturer**
Run			**Wt%**	**Wt % [a]**	**Wt%**	**Wt% [a]**
Na	0.10	Na_2O	0.13	3.5	0.05	0.3
Ca	6.31	CaO	1.09	0.8	6.02	3.4
K	4.29	K_2O	2.68	3.8	3.44	3.2
Mg	0.52	MgO	0.21	0.4	0.36	1.4
Fe	2.67	Fe_2O_3	1.07	0.7	3.63	1.6
Al	9.51	Al_2O_3	8.04	11.9	8.25	11.9
Si	76.26	SiO_2	86.25	69.1	77.94	64.9
P	0.27	P_2O_5	0.53		0.33	>0.05
		MnO		0.02		
		TiO_2		0.1		
Total			100	90.32	100	86.7

[a] Reference [31].

3.4. ^{27}Al NMR

Aluminum NMR is very sensitive to the geometry with 6-coordinate species resonating around 4–11 ppm and 4-coordinate downfield in the range 55–66 ppm depending on the nature of the aluminosilicate species [51]. Only one signal at 55 ppm belonging to tetrahedral aluminum species was evident in the ^{27}Al spectrum of a clinoptilolite found in Cuba [39]. As is evident in Figure 9, which displays the ^{27}Al NMR of the calcined NV-Na sample, the Al in that sample is composed mainly of 4-coordinate Al species, as the spectrum consists mainly of a large single resonance at 54.49 ppm. A much smaller quantity is in the octahedral conformation that corresponds to the peak at 2.60 ppm. Applying a framework equation [51], which equates the position of the ^{27}Al isotropic chemical shift to the angles on the Al (i.e., $\delta_{Al} = 132 - (0.5 \bullet \angle$Al-O-Si)), would suggest a mean $\angle$Al-O-Si of 155°. However, this derivation is not valid for zeolites with a high percentage of Si, as other factors also pertain [52].

Subjecting the zeolite to HCl resulted in changes in the ^{27}Al NMR spectrum, as evident in Figure 10. The peak for the 4-coordinate species in calcined NV-Na shifts from 54.99 to a broad peak with peaks at 53.96 and 59.64 ppm for the 30 min HCl NV-Na. Additionally, there is a slight shift in the octahedral resonance from 2.60 to 2.03 ppm. This indicates that the ratio of tetrahedral to octahedral aluminum has changed; however, it is unknown whether this is due to conversion or the dissolution of one of the forms following HCl treatment [32].

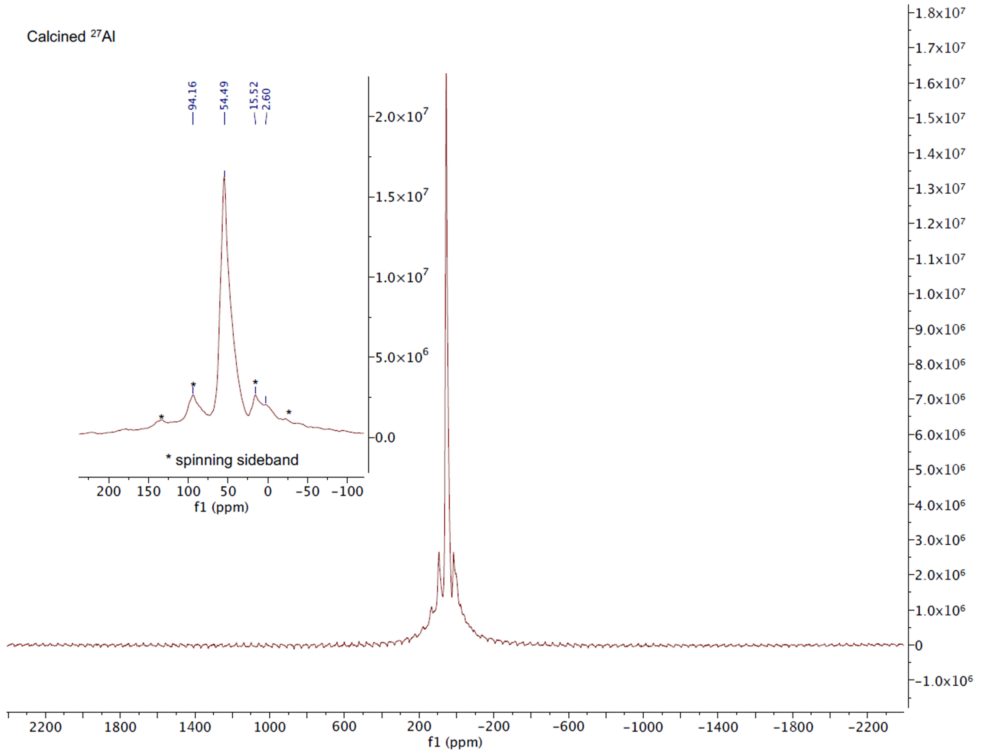

Figure 9. The ^{27}Al NMR of calcined NV-Na externally referenced to 1M $Al(NO_3)_3$ at 0.0 ppm.

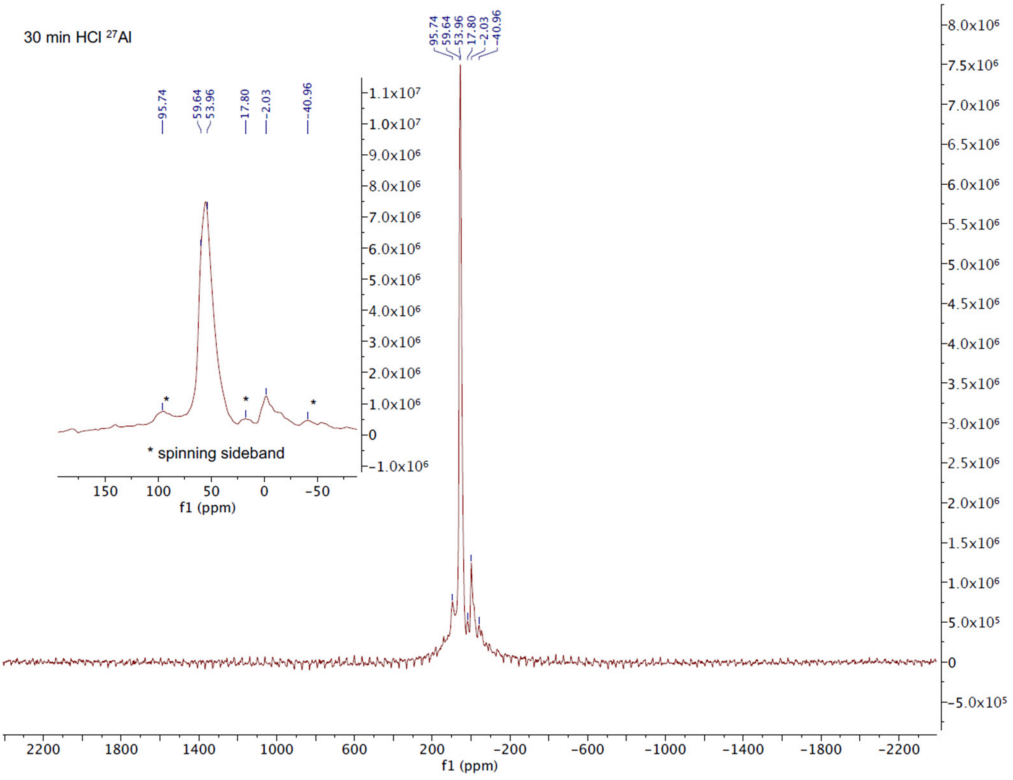

Figure 10. The ^{27}Al NMR of 30 min HCl NV-Na externally referenced to 1 M $Al(NO_3)_3$ at 0.0 ppm.

3.5. ^{29}Si MAS NMR

3.5.1. Calcined NV-Na

The ^{29}Si NMR spectrum of clinoptilolite has been reported to consists of peaks at −112.8, −106.9, and −100.6 ppm, with the peak at −106.9 ppm having the highest intensity [53]. The spectrum for calcined NV-Na contains many signals, as listed in Figure 11, but the one with the most area occurs at −106.02 ppm (27.12%). Peaks at −112.14 (13.46%) and −100.1 (23.43%) ppm are also obtained, and these are probably from the clinoptilolite regions within calcined NV-Na. Peaks at −95.99 (19.56%), −101.11 (2.48%), and −108.58 (13.90%) ppm are also evident in the deconvoluted analysis, Figure 10. The peak at −95.99 ppm may be either due to SiOH and $Si(OH)_2$ groups, as Si resonances for these groups lie in this range [53], or related to the presence of Fe^{3+} complexes rather than Al^{3+} [39]. Studies on a natural clinoptilolite from Cuba reported peaks and area percentages of −94.90 (5.7%), −97.8 (2.3%), −100.90 (34%), −106.90 (45.3%), and −112.70 (13.7%) [39]. These peaks are very close in position and area to that ascribed to a heulandite zeolite that has the following peaks and areas, −93.44 (4.25%), −98.44 (31.26%), −104.63 (56.11%), and −111.41 (8.37%) [54]. However, in our NV-Na sample, the peaks at −101.11 (2.48%) and −108.58 (13.90%) are probably due to impurities, with the one at −108.58 ppm possibly due to regions of pure $(SiO_2)_n$ [55].

The Si:Al ratio was calculated from the ^{29}Si MAS NMR data using Equation (1) [53].

$$\frac{Si}{Al} = \frac{\sum_0^4 I_{Si(nAl)}}{\sum_0^4 0.25 * nI_{Si(nAl)}} \quad (1)$$

In this equation, n represents the number of aluminum atoms connected to silicon through an oxygen bridge, and a value of 4.34 for the Si:Al ratio pertains to justify a mostly clinoptilolite designation.

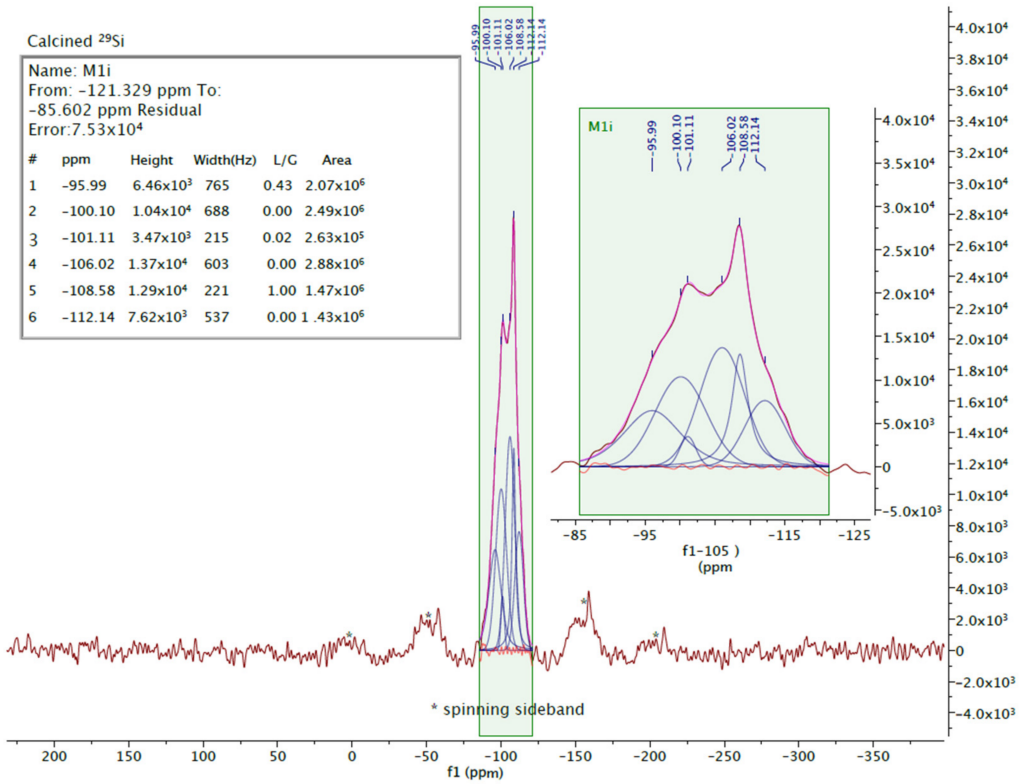

Figure 11. The 29Si NMR spectrum of calcined NV-Na referenced externally to a sample of talc at −98.1 ppm relative to tetramethylsilane (TMS) at 0 ppm. The shaded inset depicts the obtained resonances on top and the deconvoluted components of the fit below.

3.5.2. 30 min HCl NV-Na

There are dramatic changes to the ^{29}Si NMR spectrum of the 30 min HCl NV-Na, Figure 12, compared to NV-Na, Figure 11. A peak (ppm) and area percentage profile of −91.13 (1.83%), −94.01 (1.97%), −97.51 (9.25%), −102.81 (22.40%), −108.37 (39.36%) and −112.33 (25.19%) is obtained. The intense clinoptilolite peak at −106.02 present in NV-Na is no longer present, and an increase in the peak at −108.37, which was ascribed above to $(SiO_2)_n$ entities, is observed. The peaks at −91.13 and −94.01 ppm may be due to SiOH and $Si(OH)_2$ groups, and the peaks at −97.51 and −102.81 ppm correspond to silicon being connected to either one or two aluminum atoms via oxygen atom bridges [53]. As the nature of this modified zeolite is not known precisely, the Si:Al ratio cannot be assessed.

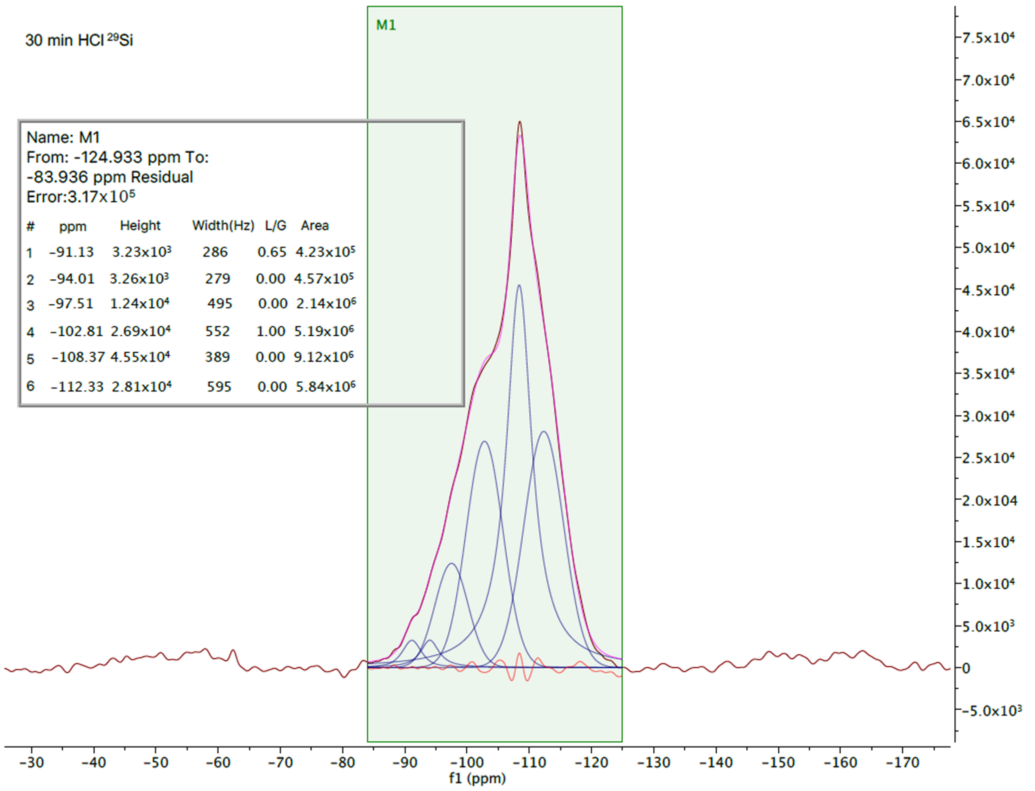

Figure 12. The ^{29}Si NMR spectrum of 30 min HCl NV-Na referenced externally to a sample of talc at −98.1 ppm relative to TMS at 0 ppm. The resonances on top are from the sample, and the deconvoluted components of the fit are below.

3.6. SEM

Scanning electron micrographs of calcined NV-Na and 30 min HCl NV-Na were obtained as presented in Figure 13. The overall morphology of calcined NV-Na looks smoother than those published at an equal magnification (i.e., 10 µm) and somewhat larger, approx. 20 µm compared to 5 µm [56]. HCl treatment results in a much less "smooth" surface comparing the images in Figure 13b for calcined NV-Na and (e) for 30 min HCL NV-Na, and there appear to be many more voids, which correlates positively with the increase in surface area measurements from the BET calculations. The 5 µm images for the samples consist of smooth surfaces, albeit with smaller particle sizes for the 30 min HCl NV-Na.

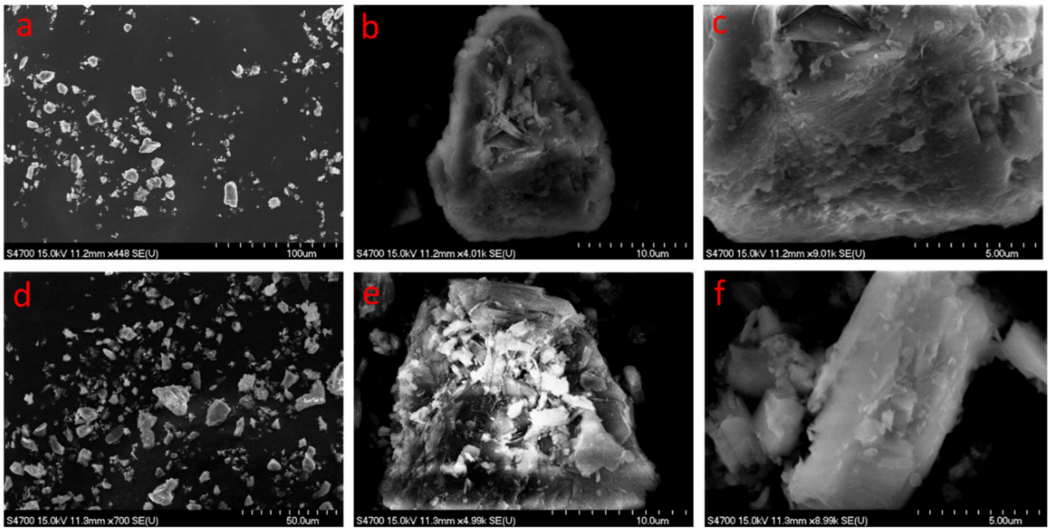

Figure 13. The SEM images of calcined NV-Na at a 100 μm scale (**a**), a 10 μm scale (**b**), and a 5 μm scale (**c**), and that of 30 min HCl NV-Na at a 50 μm scale (**d**), a 10 μm scale (**e**), and a 5 μm scale (**f**).

3.7. ATR-FTIR

The ATR-FTIR spectra for the calcined and HCl-modified clinoptilolites are displayed in Figure 14. All contain a small absorption around 1650 cm^{-1}, which has been ascribed to a deformation vibration of residual water bound up inside of the zeolite [57]. The very large broad absorption is due to stretches of the Si-O or Al-O bonds of a tetrahedral nature in the zeolite. It is noteworthy that the center of this absorption shifts from 1024 to 1071 cm^{-1} for the calcined NV-Na to 30 min HCl NV-Na. Quartz is known to have a large absorption around 1088 cm^{-1} [58], and the fact that this peak for the 30 min HCl NV-Na occurs at 1071 cm^{-1} would suggest that most of the non-Si elements were removed in the HCl treatment, leaving behind essentially porous quartz. The peaks around 795 cm^{-1} are due to the symmetric stretch of Si-O or Al-O bonds of a tetrahedral nature of the zeolite [59]. Finally, the peak that appears in calcined NV-Na at 672 cm^{-1} is indicative of an octahedral species, most likely aluminum or iron [57].

3.8. Lead Removal Study

It was of interest to compare the lead absorption and/or adsorption capacities between the calcined material and the 30 min HCl modified clinoptilolites, which had more micropores and a larger surface area. First, AZLB-Na and AZLB-Ca removed 2.05(27) and 2.00(11) meq/g of Pb^{2+}, and this was slightly more than the removal with the clinoptilolites as evident in Table 5. This difference, i.e., better removal with chabazites than clinoptilolites, was previously noted [37]. Two other natural clinoptilolites report an ion exchange of 0.730 meq/g Pb^{2+} [60], and 0.433 meq/g Pb^{2+} [61]. NV-Na calcined is significantly better at the ion exchange of Pb^{2+} than these natural clinoptilolites at 1.50(17) meq/g, Table 5. NM-Ca, 30 min HCl NV-Na, and 30 min HCl NM-Ca are not as efficient for ion exchange of Pb^{2+} with values of 0.27(14), 0.41(23), and 0.06(9) meq/g, respectively, Table 5.

The results of this lead removal study prove that treating the zeolite in HCl acid decreases the ability of the zeolite to remove lead ions from the solution. Theoretically, if the removal of lead was based on ion exchange, the Pb^{2+} ion would likely exchange with K^+ due to the radius of Pb^{2+} being 133 pm versus K^+ having a radius of 137 pm [62]. However, if lead ions are exchanged solely with K^+ ions, NM-Ca should have a higher rate of removal than NV-Na. The increase in uptake by NV-Na may be attributed to the fact that it contains less quartz than NM-Ca. Thus a more clinoptilolite structure, as was evident in the X-ray powder diffraction spectra, Figures 3 and 4.

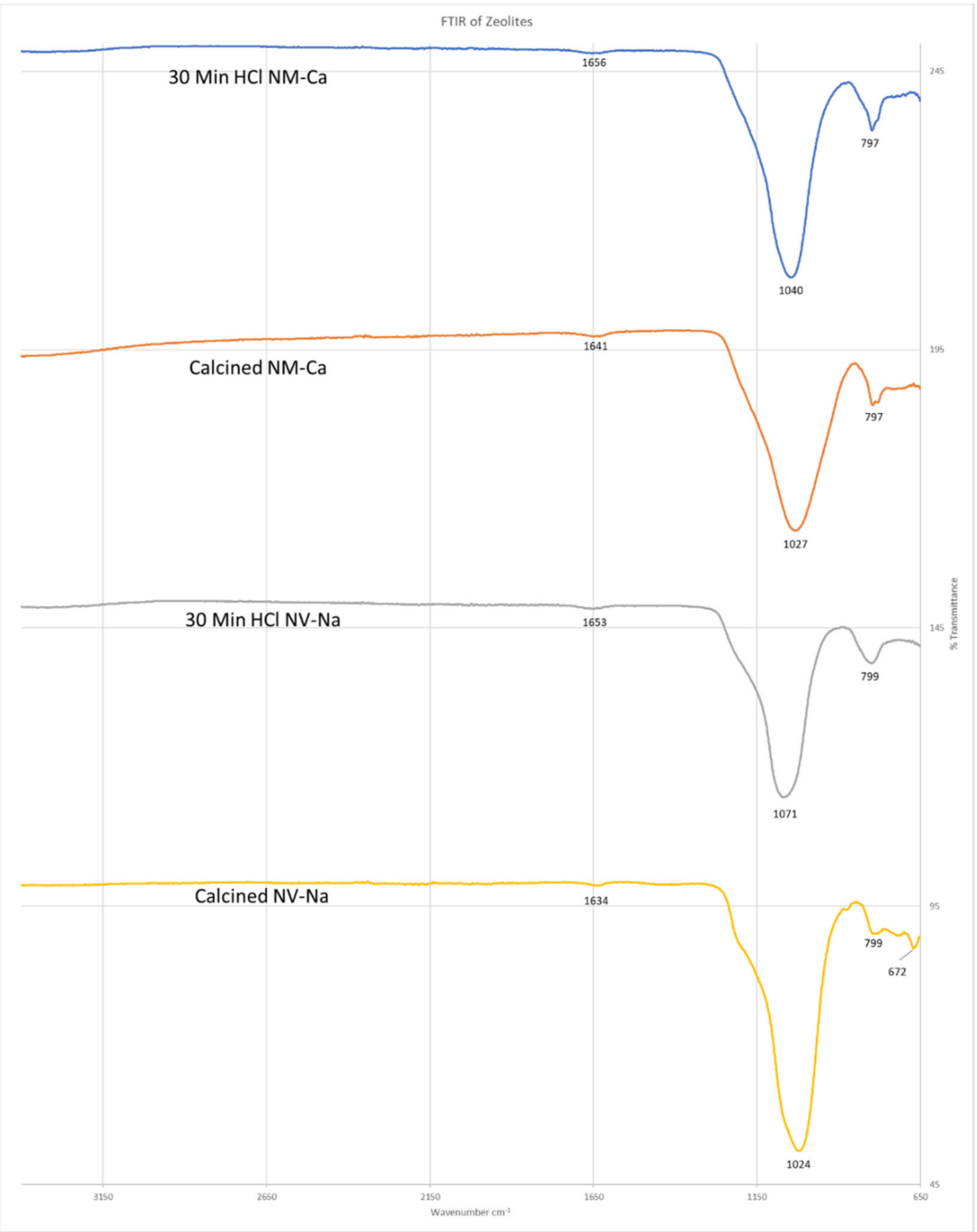

Figure 14. The ATR-FTIR spectra of Calcined NV-Na, 30 min HCl NV-Na, Calcined NM-Ca, and 30 min HCl NM-Ca.

Table 5. The Pb^{2+} removal by the zeolites at a time of 5 days at 35 °C.

Sample	Meq/g of Pb^{2+} (3 Samples)
AZLB-Na	2.05(27)
AZLB-Ca	2.00(11)
NV-Na calcined	1.50(17)
NM-Ca calcined	0.27(14)
30 min HCl NV-Na	0.41(23)
30 min HCl NM-Ca	0.06(9)

In order to increase the lead ion uptake, the zeolites (natural and modified NV-Na and NM-Ca) were stirred in a 1 M KCl solution at 25 °C for 5 days, Table 6. The solutions were

then filtered and washed with water until the filtrate was clear of chloride ions, which were monitored by tests with silver nitrate solution [63]. After drying and calcining at 550 °C for 5 h, these treated zeolites were tested similarly for their ability to remove lead ions from polluted water.

Table 6. The Pb^{2+} removal by the K^+ charged zeolites at a time of 5 days at 35 °C.

Sample	Meq/g of Pb^{2+} (3 Samples)
K^+ charged NV-Na	0.84(5)
K^+ charged NM-Ca	0.34(3)
K^+ charged 30 min HCl NV-Na	0.22(5)
K^+ charged 30 min HCl NM-Ca	0.07(9)

The results listed in Table 6 show that charging NV-Na with KCl decreased its ability to remove lead, as there was a significant decrease in the quantities removed, 1.50(17) for NV-Na calcined to 0.84(5) meq/g for the K^+ charged sample. There were no significant differences with the other zeolites, as this method did not have high enough precision, as is evident in the data in Tables 5 and 6. However, charging these zeolites with potassium ions by stirring in a potassium chloride solution was ineffective at increasing the zeolite's ability to remove Pb^{2+} ions from the solution. It is also possible, given the high percentage concentration of Si in the two zeolites, removal of the Fe^{3+} and Al^{3+} ions result in a more electrically neutral species, thus reducing the capacity for ion exchange.

4. Conclusions

The assignment of four natural zeolites, labeled AZLB-Ca, AZLB-Na, NV-Na, and NM-Ca, as containing chabazite and clinoptilolite forms were examined by X-ray powder diffraction. One of these, NM-CA turned out to be mostly quartz, namely NM-Ca. The two chabazites (AZLB-Na and AZLB-Ca) lost structural integrity after boiling in concentrated HCl acid, as is evident by the amorphous pattern generated in the powder X-ray diffraction patterns. Zeolites NV-Na and NM-Ca, which are clinoptilolites, withstood boiling in concentrated HCl acid, as can be seen by the remaining sharp peaks in their powder X-ray diffraction spectra. Results from X-ray fluorescence measurements confirmed that concentrated HCl acid was effective at removing aluminum, calcium, magnesium, sodium, potassium, and iron from the framework. These two results suggested that NM-Ca had a higher concentration of quartz impurities than NV-Na. The increase in pore size/or increase in the number of pores by removing atoms from the structure was confirmed via BET surface area analysis with NM-Ca 20.0(1) to 111(4) m^2/g and NV-Na 19.0(4) to 158(7) m^2/g. ^{29}Si and ^{27}Al MAS NMR were performed on the natural and treated NV-Na zeolite, and the data for the natural NV-Na zeolite suggested a Si:Al ratio of 4.33 similar to that determined by X-Ray fluorescence of 4.55. A lead removal study performed to determine whether the increase in pore size/or increase in the number of pores after the acid treatment would result in increased capturing of lead ions found that the acid treatment decreased the ability of the zeolite to remove lead ions from the solution. Unmodified NM-Ca removed 0.27(14), NV-Na, 1.50(17) meq/g compared to the modified zeolites, 30 min HCl treated NM-Ca 0.06(9) and NV-Na, 0.41(23) meq/g, and also decreased upon K^+ ion pretreatment in the HCl modified zeolites. Thus, increasing the surface area of the natural zeolites with concentrated HCL acid treatment was not useful at increasing cation removal or ion exchange capabilities. However, it is also possible that the removal of acid in the acid-treated zeolites was not thorough and thus, lead removal was compromised with the acid-treated samples species. These results suggest that clinoptilolites modified with this 12.1 M HCl concentrated treatment, which results in substantially larger pore sizes, may be better suited for removing neutral contaminants from solution or as 3-dimensional hollow structures to allow for slow release of fertilizers in soil treatment.

Author Contributions: Conceptualization, R.L.L.; methodology, R.L.L. and N.K.N.; formal analysis, N.K.N. and R.L.L.; investigation, G.M.H. and N.K.N.; resources, R.L.L. and M.E.M.; data curation, G.M.H. and N.K.N.; writing—original draft preparation, N.K.N. and R.L.L.; writing—review and editing, R.L.L., N.N, G.M.H., and M.E.M.; visualization, N.K.N. and R.L.L.; supervision, R.L.L.; project administration, R.L.L. and N.K.N. All authors have read and agreed to the published version of the manuscript.

Funding: This research received no external funding.

Institutional Review Board Statement: Not applicable.

Informed Consent Statement: Not applicable.

Acknowledgments: Special thanks to Jared Edwards for obtaining the SEM images, Edward Laitila for assistance with the XRF measurements, and Daniel Holmes of the Max T. Rogers NMR Facility at Michigan State University for the solid-state NMR spectra. The zeolites were generously donated by the St. Cloud Mining Company. Michigan Technological University is acknowledged for its support. Insightful comments from reviewers are acknowledged.

Conflicts of Interest: The authors declare no conflict of interest.

References

1. Virta, R.L. Zeolites. In *U.S. Geological Survey Minerals Yearbook*; United States Government, Department of the Interior: Washington, DC, USA, 2001; pp. 1–5.
2. Smith, J.V. Origin and structure of zeolites. *ACS Monogr.* **1976**, *171*, 3–79.
3. Funada, S.; Omi, T.; Nakamura, K.; Sasagawa, S.; Tanaka, M.; Igarashi, K.; Abe, T.; Obata, K.; Sasaki, S. Fired Zeolites Useful for Construction Materials, Direct-Heat Cooking Utensils, and Warm Rock Bathtubs. Japanese Patent JP2007320807; Fukuda Corp., 13 December 2007.
4. Yorukogullari, E. A Novel Ecological and Biological Organomineral Fertilizer. Turkish Patent WO2019212440, 21 November 2019.
5. Song, H.; Guo, W.; Liu, J. Compound Fertilizer and Its Preparation Method. Chinese Patent CN108083950, 29 May 2018.
6. Zhu, J.; Zhang, X. Functional Soil Conditioning Agent and Preparation Method Thereof. Chinese Patent CN107056557, 18 August 2017.
7. Meng, F.; Yang, L. Fertilizer Containing Seaweed Extract and Preparation Method Thereof. Chinese Patent CN106854107, 16 June 2017.
8. Jin, Z.; Zhang, Y.; Xu, W.; Lai, N. Special Slow Release Water-Soluble Fertilizer Used for Grape. Chinese Patent CN106396868, 15 February 2017.
9. Chen, Q.; Zeng, J. Controlled-Release Phosphorus Fertilizer Using ph Sensitive Material and Preparation Method Thereof. Chinese Patent CN104387161, 4 March 2015.
10. Jin, W.; Meng, X. Zeolite Sustained-Release Fertilizer and Its Manufacturing Method. Chinese Patent CN103304311, 18 September 2013.
11. Merchant, R.J.; Chan, P.L.S.; Ashenden, P.J. Improvements in or Relating to Cleaning or Cosmetic Compositions Comprising Natural Zeolites. World Intellectual Property Organization WO2010082847, 22 July 2010.
12. Herzog, C.; Hraschan, J.; Lelas, A. Use of Zeolites for Reducing the Proportion of Lactates and Ammonium in Human and Animal Organisms. World Intellectual Property Organization WO2003072116, 4 September 2003.
13. Barlokova, D.; Ilavsky, J. Natural zeolites with a surface mno2 layer for water treatment. *Chem. Listy* **2014**, *108*, 1153–1157.
14. Mumpton, F.A. *La roca magica*: Uses of natural zeolites in agriculture and industry. *Proc. Natl. Acad. Sci. USA* **1999**, *96*, 3463. [CrossRef] [PubMed]
15. Szerement, J.; Szatanik-Kloc, A.; Jarosz, R.; Bajda, T.; Mierzwa-Hersztek, M. Contemporary applications of natural and synthetic zeolites from fly ash in agriculture and environmental protection. *J. Clean. Prod.* **2021**, *311*, 127461. [CrossRef]
16. Wen, J.; Dong, H.; Zeng, G. Application of zeolite in removing salinity/sodicity from wastewater: A review of mechanisms, challenges and opportunities. *J. Clean. Prod.* **2018**, *197*, 1435–1446. [CrossRef]
17. Krstic, V.; Urosevic, T.; Pesovski, B. A review on adsorbents for treatment of water and wastewaters containing copper ions. *Chem. Eng. Sci.* **2018**, *192*, 273–287. [CrossRef]
18. Chojnacka, M.; Sobolewska, P.; Petrus, R.; Warchol, J. Cr(vi) sorption on surface-modified natural zeolites. *Przem. Chem.* **2017**, *96*, 332–337.
19. Ates, A.; Akgül, G. Modification of natural zeolite with naoh for removal of manganese in drinking water. *Powder Technol.* **2016**, *287*, 285–291. [CrossRef]
20. Zhao, Y. Review of the natural, modified, and synthetic zeolites for heavy metals removal from wastewater. *Environ. Eng. Sci.* **2016**, *33*, 443–454.
21. Wang, K. Method and regeneration of sodium modified zeolites for treatment of ammonia-nitrogen wastewater. *Shuichuli Jishu* **2016**, *42*, 118–120.

22. Shi, H.; Wei, L.; Yan, C.; Li, X. Research progress of phosphorus removal by zeolite in wastewater. *Guangdong Huagong* **2014**, *41*, 165–169.
23. Regmi, U.; Boyer, T.H. Ammonium and potassium removal from undiluted and diluted hydrolyzed urine using natural zeolites. *Chemosphere* **2021**, *268*, 128849. [CrossRef]
24. Zwain, H.M.; Vakili, M.; Dahlan, I. Waste material adsorbents for zinc removal from wastewater: A comprehensive review. *Int. J. Chem. Eng.* **2014**, *2014*, 347912. [CrossRef]
25. Sukmasari, E.; Azmiyawati, C. Modification of natural zeolite with Fe(iii) and its application as adsorbent chloride and carbonate ions. *IOP Conf. Ser. Mater. Sci. Eng.* **2018**, *349*, 012075.
26. Armbruster, T.; Gunter, M.E. Crystal structures of natural zeolites. *Rev. Mineral. Geochem.* **2001**, *45*, 1–67. [CrossRef]
27. Ambrozova, P.; Kynicky, J.; Urubek, T.; Nguyen, V.D. Synthesis and modification of clinoptilolite. *Molecules* **2017**, *22*, 1107. [CrossRef]
28. Ruíz-Baltazar, A.; Esparza, R.; Gonzalez, M.; Rosas, G.; Pérez, R. Preparation and characterization of natural zeolite modified with iron nanoparticles. *J. Nanomater.* **2015**, *2015*, 364763. [CrossRef]
29. Wani, A.L.; Ara, A.; Usmani, J.A. Lead toxicity: A review. *Interdiscip. Toxicol.* **2015**, *8*, 55–64. [CrossRef]
30. Coombs, D.S.; Alberti, A.; Armbruster, T.; Artioli, G.; Colella, C.; Galli, E.; Grice, J.D.; Liebau, F.; Mandarino, J.A.; Minato, H.; et al. Recommended nomenclature for zeolite minerals: Report of the subcommittee on zeolites of the international mineralogical association, commission on new minerals and mineral names. *Can. Miner.* **1997**, *35*, 1571–1606.
31. St. Cloud Mining Company. Available online: https://www.stcloudmining.com/sales/data-sheets-applications/ (accessed on 4 June 2021).
32. Thrush, K.A.; Kuznicki, S.M. Characterization of chabazite and chabazite like zeolites of unusual composition. *J. Chem. Soc. Faraday Trans.* **1991**, *87*, 1031–1035. [CrossRef]
33. Kuznicki, S.M.; Lin, C.C.H.; Bian, J.; Anson, A. Chemical upgrading of sedimentary na-chabazite from bowie, arizona. *Clays Clay Miner.* **2007**, *55*, 235–238. [CrossRef]
34. Yazdanbakhsh, F.; Alizadehgiashi, M.; Sawada, J.A.; Kuznicki, S.M. A clinoptilolite-pdms mixed-matrix membrane for high temperature water softening. *Water Sci. Technol.* **2016**, *73*, 1409–1417. [CrossRef] [PubMed]
35. An, W.; Zhou, X.; Liu, X.; Chai, P.W.; Kuznicki, T.; Kuznicki, S.M. Natural zeolite clinoptilolite-phosphate composite membranes for water desalination by pervaporation. *J. Membr. Sci.* **2014**, *470*, 431–438. [CrossRef]
36. Adamaref, S.; An, W.; Jarligo, M.O.; Kuznicki, T.; Kuznicki, S.M. Natural clinoptilolite composite membranes on tubular stainless steel supports for water softening. *Water Sci. Technol.* **2014**, *70*, 1412–1418. [CrossRef] [PubMed]
37. Kesraoui-Ouki, S.; Cheeseman, C.; Perry, R. Effects of conditioning and treatment of chabazite and clinoptilolite prior to lead and cadmium removal. *Environ. Sci. Technol.* **1993**, *27*, 1108–1116. [CrossRef]
38. Jang, H.K.; Chung, Y.-D.; Whangbo, S.W.; Lyo, I.W.; Whang, C.N.; Lee, S.J.; Lee, S. Effects of chemical etching with hydrochloric acid on a glass surface. *J. Vacuum Sci. Technol. A Vacuum Surf. Films* **2000**, *18*, 2563–2567. [CrossRef]
39. Garcia-Basabe, Y.; Rodriguez-Iznaga, I.; de Menorval, L.-C.; Llewellyn, P.; Maurin, G.; Lewis, D.W.; Binions, R.; Autie, M.; Ruiz-Salvador, A.R. Step-wise dealumination of natural clinoptilolite: Structural and physicochemical characterization. *Microporous Mesoporous Mater.* **2010**, *135*, 187–196. [CrossRef]
40. Tišler, Z.; Hrachovcová, K.; Svobodová, E.; Šafář, J.; Pelíšková, L. Acid and thermal treatment of alkali-activated zeolite foams. *Minerals* **2019**, *9*, 719. [CrossRef]
41. Brunauer, S.; Emmett, P.H.; Teller, E. Adsorption of gases in multimolecular layers. *J. Am. Chem. Soc.* **1938**, *60*, 309–319. [CrossRef]
42. Altomare, A.; Corriero, N.; Cuocci, C.; Falcicchio, A.; Moliterni, A.; Rizzi, R. Qualx2.0: A qualitative phase analysis software using the freely available database pow_cod. *J. Appl. Cryst.* **2015**, *48*, 598–603. [CrossRef]
43. O'Neill, L. Icdd annual spring meetings. *Powder Diffr.* **2013**, *28*, 137–148. [CrossRef]
44. Abuyaghi, A.; El-Bishtawi, R. Removal of lead and nickel ions using zeolite tuff. *J. Chem. Technol. Biotechnol.* **1997**, *69*, 27–34.
45. Treacy, M.M.J.; Higgins, J.B. (Eds.) *Collection of Simulated Xrd Powder Patterns for Zeolites*; Elsevier: Amsterdam, The Netherlands, 2001; p. 586.
46. Keller, E.B.; Meier, W.M.; Kirchner, R.M. Synthesis, structures of alpo4-c and alpo4-d, and their topotactic transformation. *Solid State Ionics* **1990**, *43*, 93–102. [CrossRef]
47. Galli, E.; Gottardi, G.; Mayer, H.; Preisinger, A.; Passaglia, E. The structure of potassium-exchanged heulandite at 293, 373 and 593 k. *Acta Crystallogr. Sect. B Struct. Sci.* **1983**, *39*, 189–197. [CrossRef]
48. Koyama, K.; Takeuchi, Y. Clinoptilolite: The distribution of potassium atoms and its role in thermal stability. *Z. Kristallogr. Cryst. Mater.* **1977**, *145*, 216–239. [CrossRef]
49. Levien, L.; Prewitt, C.T.; Weidner, D.J. Structure and elastic properties of quartz at pressure. *Am. Miner.* **1980**, *65*, 920–930.
50. Arletti, R.; Quartieri, S.; Vezzalini, G. Elastic behavior of zeolite boggsite in silicon oil and aqueous medium: A case of high-pressure-induced over-hydration. *Am. Miner.* **2010**, *95*, 1247–1256. [CrossRef]
51. Lippmaa, E.; Samoson, A.; Magi, M. High-resolution aluminum-27 nmr of aluminosilicates. *J. Am. Chem. Soc.* **1986**, *108*, 1730–1735. [CrossRef]
52. Holzinger, J.; Nielsen, M.; Beato, P.; Brogaard, R.Y.; Buono, C.; Dyballa, M.; Falsig, H.; Skibsted, J.; Svelle, S. Identification of distinct framework aluminum sites in zeolite zsm-23: A combined computational and experimental 27al nmr study. *J. Phys. Chem. C* **2019**, *123*, 7831–7844. [CrossRef]

53. Lippmaa, E.; Maegi, M.; Samoson, A.; Tarmak, M.; Engelhardt, G. Investigation of the structure of zeolites by solid-state high-resolution silicon-29 nmr spectroscopy. *J. Am. Chem. Soc.* **1981**, *103*, 4992–4996. [CrossRef]
54. Khodabandeh, S.; Davis, M.E. Synthesis of a heulandite-type zeolite by hydrothermal conversion of zeolite p1. *Chem. Commun.* **1996**, 1205–1206. [CrossRef]
55. Malfait, W.J.; Halter, W.E.; Verel, R. 29si nmr spectroscopy of silica glass: T1 relaxation and constraints on the si–o–si bond angle distribution. *Chem. Geol.* **2008**, *256*, 269–277. [CrossRef]
56. Minceva, M.; Fajgar, R.; Markovska, L.; Meshko, V. Comparative study of Zn^{2+}, Cd^{2+}, and Pb^{2+} removal from water solution using natural clinoptilolitic zeolite and commercial granulated activated carbon. Equilibrium of adsorption. *Sep. Sci. Technol.* **2008**, *43*, 1–27. [CrossRef]
57. Zendelska, A.; Golomeova, M.; Jakupi, Š.; Lisichkov, K.; Kuvendziev, S.; Marinkovski, M. Characterization and application of clinoptilolite for removal of heavy metal ions from water resources. *Geol. Maced.* **2018**, *32*, 21–32.
58. Shahack-Gross, R.; Bar-Yosef, O.; Weiner, S. Black-coloured bones in hayonim cave, israel: Differentiating between burning and oxide staining. *J. Archaeol. Sci.* **1997**, *24*, 439–446. [CrossRef]
59. Akdeniz, Y.; Ülkü, S. Thermal stability of ag-exchanged clinoptilolite rich mineral. *J. Therm. Anal. Calorim.* **2008**, *94*, 703–710. [CrossRef]
60. Oter, O.; Akcay, H. Use of natural clinoptilolite to improve water quality: Sorption and selectivity studies of lead(ii), copper(ii), zinc(ii), and nickel(ii). *Water Environ. Res.* **2007**, *79*, 329–335. [CrossRef] [PubMed]
61. Inglezakis, V.J.; Loizidou, M.D.; Grigoropoulou, H.P. Equilibrium and kinetic ion exchange studies of Pb^{2+}, Cr^{3+}, Fe^{3+} and Cu^{2+} on natural clinoptilolite. *Water Res.* **2002**, *36*, 2784–2792. [CrossRef]
62. Shannon, R. Revised effective ionic radii and systematic studies of interatomic distances in halides and chalcogenides. *Acta Crystallogr. Sect. A* **1976**, *32*, 751–767. [CrossRef]
63. Santiago, O.; Walsh, K.; Kele, B.; Gardner, E.; Chapman, J. Novel pre-treatment of zeolite materials for the removal of sodium ions: Potential materials for coal seam gas co-produced wastewater. *SpringerPlus* **2016**, *5*, 571. [CrossRef]